International Journal of Naval Architecture and Ocean Engineering 15 (2023) 100544

Contents lists available at ScienceDirect

International Journal of Naval Architecture and Ocean Engineering

journal homepage: http://www.journals.elsevier.com/international-journal-of-naval-architecture-and-ocean-engineering/

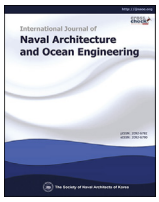

Moored motion prediction of a semi-submersible offshore platform in waves using an OpenFOAM and MoorDyn coupled solver

Wooyoung Jeon [a], Sunho Park [b, *], Seokkyu Cho [c]

[a] Department of Convergence Studies on the Ocean Science and Technology, Korea Maritime and Ocean University, Busan, Republic of Korea
[b] Department of Ocean Engineering, Korea Maritime and Ocean University, Busan, Republic of Korea
[c] Korea Research Institute of Ships and Ocean Engineering (KRISO), Daejeon, Republic of Korea

ARTICLE INFO

Article history:
Received 10 April 2023
Received in revised form
27 July 2023
Accepted 2 August 2023
Available online 5 August 2023

Keywords:
Openfoam
MoorDyn
Semi-submersible
Moored motion
Mooring tension

ABSTRACT

In this study, the motions of a moored buoy and its surrounding fluid flow are numerically studied. The solver is developed by coupling the computational fluid dynamics platform, OpenFOAM, with a lumped mass mooring line model, MoorDyn. The time marching interface to transfer the solution variables is developed for the robustness and accuracy of the solver. The developed coupled solver was validated against a moored cubic-shaped box model in waves. The different mesh configurations, mesh generation technique and mooring line discretization are considered in the numerical study. A cubic-shaped box attached with tensioned mooring lines in waves is simulated and the results are compared with the experimental results. Motion responses of a moored semi-submersible platform, which is designed by Korea Research Institute of Ship and Ocean Engineering (KRISO), in waves are predicted by the solver. The mooring line tensions acting on the body and anchor, the forces acting on the platform and the platform's motion performance are analyzed, and comparisons are made between simulation data and experimental data.

1. Introduction

For larger offshore platforms with deep installation positions, the mooring system becomes even more important than for smaller platforms. An offshore platform is exposed to severe environmental conditions such as winds, waves, and currents, which can induce large platform motions and loads on the mooring lines. As the platform installation depth becomes deep, it requires the mooring lines to be long that resulting in large loads on the mooring line due to current and its inertia. The safety of the platform depends on the capability of the mooring system to withstand these loads, therefore the mooring system is one of the important design factors of offshore platforms. The experiments on the offshore platform have some problems such as the limitation of water depth, wave-making capability, wave absorptions, circulating currents and scaling effects. And significant time and cost are required for the model test, and it is also very difficult to reserve the model test facilities due to their experimental schedule. One of the alternative solutions is the numerical methodology. Two numerical methods which are the potential flow-based methods and Computational Fluid Dynamics (CFD) are mainly used to analyze the offshore platform in waves. On the other hand, the CFD can model complex flow phenomena without difficulty.

The most widely used method for mathematically modeling a mooring line is the quasi-static model (Hall et al., 2011; Hall and Goupee, 2015). The quasi-static method assumes that the forces affecting the mooring line are in a state of equilibrium, e.g. no inertia forces are taken into account. The forces acting on the mooring line include external forces such as winds, waves, and currents, as well as internal forces such as the tension of the mooring line. This method can be applied to the cases when motions of a floating body connected to the mooring lines are slowly varying and the displacement of lines is small. Dynamic models can be applied to cases where the amplitude of motion is large. The dynamic models can be categorized into a lumped-mass model (Khan and Ansari, 1986) and Finite Element Method (FEM) (Aamo and Fossen, 2000). The lumped mass model treats mooring lines as a series of discrete masses connected by springs and dampers, which represents the stiffness and damping of the line, respectively. The lumped mass model-based solvers are usually used for

* Corresponding author.
E-mail address: spark@kmou.ac.kr (S. Park).
Peer review under responsibility of The Society of Naval Architects of Korea.

https://doi.org/10.1016/j.ijnaoe.2023.100544

moored body options. Thomsen et al. (2017) evaluated two pieces of commercial software, Orcaflex and DeepC. Hall and Goupee (2015) developed a solver using a lumped mass method with Runge-Kutta 2nd-order time integration method and opened it to public.

Ghafari and Dardel (2018) studied the dynamic response of the moored semi-submersible platform using AQWA. Rinaldi et al. (2021) predicted the behavior of the modular mooring system using the Orcaflex and compared these results with experimental data. Amaechi et al. (2022) conducted analyses of a moored semi-submersible platform using AQWA for hydrodynamics and Orcaflex for mooring dynamics. Yang et al. (2021) investigated mooring breakage effects of a barge-type platform using AQWA and FAST. Liu et al. (2017) coupled OpenFOAM and a quasi-static mooring model for floating offshore wind turbines. Tian et al. (2021) studied motions of a semi-submersible with a spring-type mooring system in waves. Huang et al. (2022) investigated the mooring configuration of a cylindrical buoy using the finite analytic Navier-Stokes (FANS) CFD method and in-house FEM code, MOORING3D. Kwon and Yeon (2023) simulated moored ships in confined waterway using Siemens STAR-CCM + ver. 15.06R8. To simulate moored floating body motions, a coupled solver of OpenFOAM and MoorDyn was used (Lee et al., 2021; Chen and Hall, 2022; Jiang and el Moctar, 2022; Aliyar et al., 2022). Palm et al. (2016) coupled OpenFOAM and Moody, which was an in-house dynamic model developed to capture and resolve the snap loads. Domínguez et al. (2019) coupled DualSPHysics, a Smoothed Particle Hydrodynamics (SPH) solver, and MoorDyn. Lee et al. (2021) used a loose coupling technique to couple the different times of OpenFOAM and MoorDyn. The time-delay coupling technique by Lee et al. (2021) used the position and velocity of platform from the previous time step to calculate the tension and restoring forces on the mooring system in the present time step. This approach can cause numerical errors. In this research, the motions of a moored floating body are analyzed by the advanced coupling of OpenFOAM (Jasak, 2009) and MoorDyn based on the approach of Lee et al. (2021).

The objectives of the present study are (1) to revise the coupling method to overcome inaccuracies caused by the delayed coupling in the previously developed solver and (2) to apply the enhanced time marching method to a semi-submersible platform designed by the Korea Research Institute of Ship and Ocean Engineering (KRISO). Compared with the previous research by Lee et al. (2021), the present study used the position and velocity of platform at the current time step is used to update the mooring system. Based on an improved time marching solver, dynamic analysis of the moored semi-submersible platform in waves is carried out. The simulated results are compared to the data obtained from the experiment.

2. Computational methods

2.1. Governing equations

The assumption of incompressible fluid is used to describe the flow around the floating body. The mass and momentum conservation laws are given below:

$$\nabla \bullet \left(\rho_m \overrightarrow{v}_m\right) = 0 \tag{1}$$

$$\frac{\partial \rho_m \overrightarrow{v}_m}{\partial t} + \nabla \bullet \left(\rho_m \overrightarrow{v}_m \overrightarrow{v}_m\right) = -\nabla p + \nabla \bullet \overline{\overline{\tau}} + S \tag{2}$$

where $\overrightarrow{v}, p,$ and $\overline{\overline{\tau}}$ are the velocity vector, pressure, and viscous stress tensor, respectively. S is the source term. The subscript m indicates the mixture phase. The properties of the mixture of air and water can be represented as

$$\rho_m = (1-\alpha)\rho_{air} + \alpha\rho_{water} \tag{3}$$

$$\mu_m = (1-\alpha)\mu_{air} + \alpha\mu_{water} \tag{4}$$

where ρ is the density and μ is the viscosity. α is bounded between 0 and 1, and refers to the volume fraction of water within the control volume. The subscript $''air''$ indicates the air phase and the subscript $''water''$ indicates the water phase.

To capture the interface between air-water phases, the volume fraction transport equation is used, which is expressed as follows:

$$\frac{\partial}{\partial t}(\alpha\rho_m) + \nabla \bullet \left(\alpha\rho_m \overrightarrow{v}_m\right) + C_{ad}\nabla \bullet \left(\alpha(1-\alpha)\overrightarrow{v}_r\right) = 0 \tag{5}$$

where the last term is introduced artificially to reduce the smearing of the volume fraction near the interface, and C_{ad} is the anti-diffusion coefficient. C_{ad} of 1 was used for this study (Kim and Park, 2021; Liu and Park, 2023). The relative interface normal velocity is used as the artificial compression velocity $\overrightarrow{v}_r$ as the below:

$$\overrightarrow{v}_r = \left|\overrightarrow{v}_m\right| \frac{\nabla\alpha}{|\nabla\alpha|} \tag{6}$$

2.2. Numerical methods

The Crank-Nicolson scheme with an off-centering coefficient of 0.9 is used to discretize the time derivative term. The adjustable time step size controlled by a maximum Courant number of 0.9 is used for time integration. Euler's method is used to evaluate the solution gradients at the cell centers. A Total Variation Diminishing (TVD) scheme and the van Leer limiter are used to discretize the convection terms. To discretize the diffusion terms, a central differencing scheme is used. For the velocity and pressure coupling, the PIMPLE algorithm, which is combination of the Semi-Implicit Method for Pressure Linked Equation (SIMPLE) algorithm and the Pressure-Implicit with Splitting of Operators (PISO) algorithm, is used. The number of iterations for internal loops is 2, and for external loops is 3. For the turbulence closure, the Shear Stress Transport (SST) k-ω turbulence model is adopted with the wall function in Park et al. (2013). The Gauss-Seidel method is used to solve the discretized algebraic equations, with an additional algebraic multi-grid method (Weiss et al., 1999) applied to accelerate the convergence of the solution.

2.3. Wave generation and absorption

The wave generation and absorption library which is called waves2Foam in the OpenFOAM framework is used to generate waves. The relaxation zone technique is applied to absorb reflection waves. The explicit approach in the relaxation zones is simply written as:

$$\varphi = (1-w_R)\varphi_{target} + w_R\varphi_{computed}\# \tag{7}$$

where φ is the calculated value in the relaxation zone, which can be $\overrightarrow{v}_m$ or α. The subscripts $''target''$ and $''computed''$ indicate the value from wave theory and the value from the governing equations, respectively. w_R is the weighting function, and can be written as follows:

$$w_R = 1 - \frac{\exp\left(\sigma^{3.5}\right) - 1}{\exp(1) - 1}\# \tag{8}$$

where σ is the local coordinates in the relaxation zone. σ is set to 1 and 0 at the entrance and end of the relaxation zone (Choi et al., 2023).

2.4. Mooring system modeling

MoorDyn is chosen to analyze the mooring system (Hall and Goupee, 2015). In the previous study (Lee et al., 2021), a coupled solver between OpenFOAM and MoorDyn was developed. In this old solver, the delayed coupling method is used at the interface between two solvers. At the interface, the platform's center of gravity position (x), velocity (v), and time step size (Δt) are transferred from OpenFOAM to MoorDyn to calculate the restoring force due to the mooring system. In the delayed coupling method, x uses the value at the previous-previous time step $(i-2)$, and v uses linearly calculated value from previous-previous time step $(i-2)$ and previous time step $(i-1)$, as shown in the following equation.

$$v_{i-1\frac{1}{2}} = \frac{x_{i-2} - x_{i-1}}{t_{i-2} - t_{i-1}} \tag{9}$$

where i is the time index. This method has limitations in that the accuracy is decreased when the time step size at each time step is not constant, or the platform's motion is nonlinear. In this study, the interface of the coupled solver is improved using the current time step, position, and velocity of the body. Fig. 1 shows the old and new interfaces of the solver. The improvement enables accurate predictions of the restoring force even in cases where the platform's motion is nonlinear, and the time step size varies, making it possible to use an adjustable time step size controlled by a maximum Courant number. In OpenFOAM code structure, there are some differences. The previous study has an inconvenient procedure for creating a new solver by modifying an existing OpenFOAM solver, such as *interFoam*, to couple OpenFOAM and MoorDyn. In the present study, the six degrees of freedom (6-DOF) motion library, *sixDoFRigidBodyMotionSolver* class, is revised to transfer solutions variables between OpenFOAM and MoorDyn. The variables used in MoorDyn are defined in the library and the functions of MoorDyn called in the motion library. Thus, the compatibility with existing solvers has been improved by enabling the coupling analysis of OpenFOAM and MoorDyn without creating an ad-hoc solver. Fig. 2 shows the maximum Courant number during the simulations using the new solver and old solver. The time step size during the simulation is fixed at 0.001 s to calculate the maximum Courant number. The peak value of the maximum Courant number in the simulations using the new solver is smaller than that using the old solver. This demonstrates that the improved time marching interface in the new solver performs a more numerically stable simulation.

3. Results and discussion

3.1. Moored cubic-shaped box in waves

To validate the motions of a floating body and tensile loads of the mooring system, moored motions of a floating cubic-shaped box in waves are simulated and compared with the experimental data (Wu et al., 2019). The experiments are conducted in a wave flume of the Coastal Engineering Research Group at the Department of Civil Engineering of Ghent University with a length of 30 m,

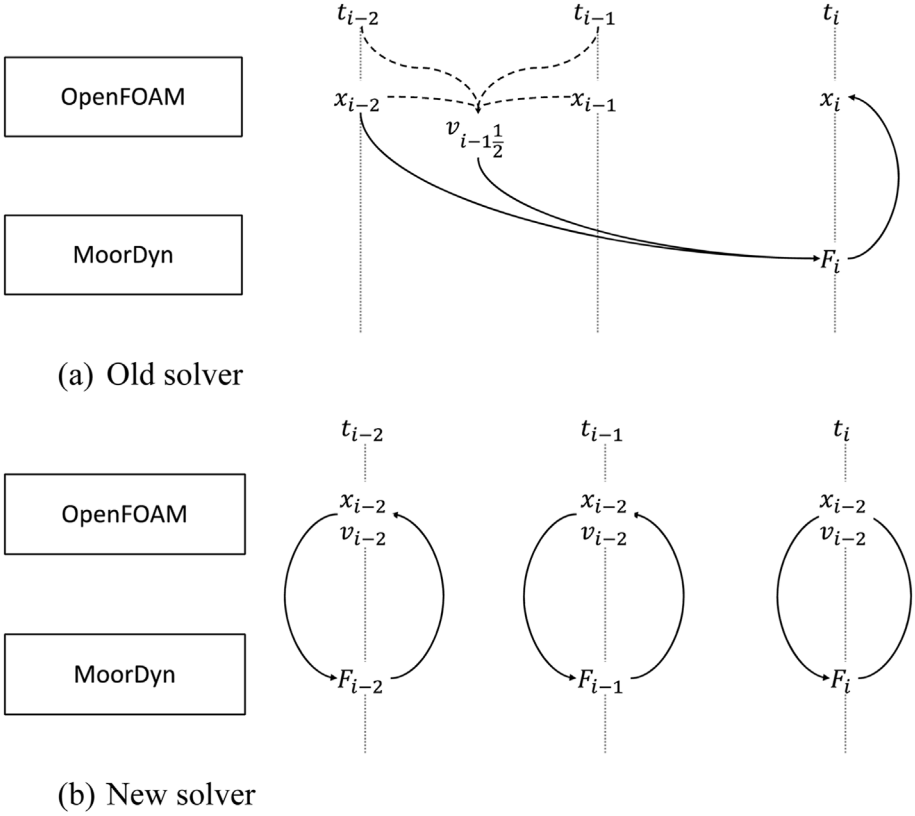

Fig. 1. Coupling interface between OpenFOAM and MoorDyn.

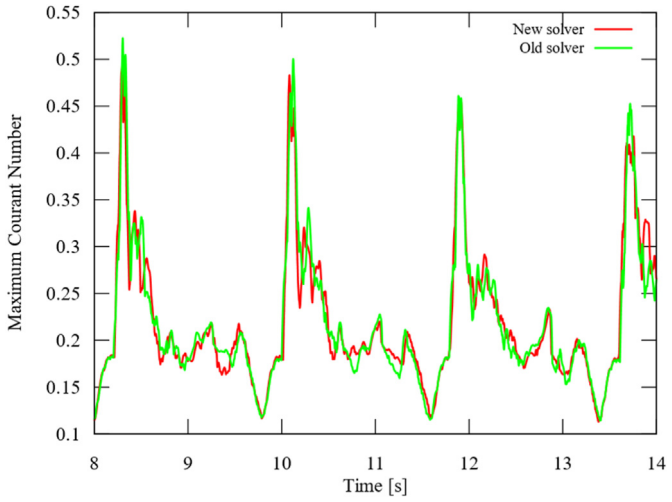

Fig. 2. Maximum Courant number using new and old solvers.

a width of 1 m, and a depth of 1.2 m, and the water depth is 0.5 m. The wave flume has a wave generator and a wave absorption beach at both ends. The wavelength of the regular waves considered is 3.57 m, the wave height is 0.12 m and the wave period is 1.8 s. Fig. 3 shows the grid system for the simulations of the floating body and the geometry of mooring lines. The geometric characteristics of the body are listed in Table 1. The center of mass is in the geometrical center of the floating cubic-shaped box.

A four-point symmetric slack mooring system is used in the experiments. Mooring lines 1 and 2 are mounted to the front of the cubic-shaped box and lines 3 and 4 are mounted to the back. The iron chain is used as the mooring line. The parameters of the mooring line are listed in Table 2.

The moving wall boundary condition is applied to the cubic-shaped box surface. For the inlet and outlet boundaries, the relaxation zone technique is applied to generate regular waves and prevent reflection waves, respectively. For the top boundary, open atmosphere condition is applied, which switched between Neumann boundary condition when the fluid is flowing out of the domain, and Dirichlet boundary condition when the fluid is flowing into the domain. For the bottom and side boundaries, no-slip boundary condition w is as applied.

Three different mesh types are considered: coarse mesh, medium mesh, and fine mesh. The resolution of the medium mesh is 80 cells per wavelength in the x-direction, which is the propagation direction of the wave, and 20 cells per wave height in the z-direction, which is the direction of gravity acceleration. This is a higher grid resolution level than the grid resolution level suggested in the ITTC guideline (ITTC, 2014), which is recommended 40 cells per wavelength and 20 cells per wave height (hereinafter referred to as "medium mesh"). The coarse and fine meshes has half and twice the number of meshes used in the medium mesh, respectively. To examine the effect of grid convergence, simulations are performed with the coarse, medium, and fine meshes. Two types of mesh deformation techniques, the morphing mesh and the overset mesh, are considered for the movement of the floating body. The morphing mesh technique is a traditional technique in which the meshes around it changes when the body has motions. The overset mesh technique depicts motions by exchanging data in two independent meshes without mesh deformation. For a large motion, overset mesh is widely used.

In the lumped-mass model, the mooring line is present by connecting several segments. For the mooring line segment count,

Table 1
Geometric characteristics of the floating cubic-shaped body.

Properties of cubic-shaped box	Value	Unit
Length (x-direction)	0.2	m
Width (y-direction)	0.2	m
Height (z-direction)	0.132	m
Draft	0.079	m
Mass	3.148	kg
Mooring line fairlead height from bottom	0.005	m
Moment of inertia of x-axis	0.015	kg • m^2
Moment of inertia of y-axis	0.015	kg • m^2
Moment of inertia of z-axis	0.021	kg • m^2

Table 2
Parameters of mooring line.

Properties	Value	Unit
Horizontal span	1.385	m
Vertical span	0.420	m
Total length of the mooring line	1.455	m
Line diameter	3.57	mm
Line weight	0.06	kgf/m
Axial stiffness (*EA*)	29	N

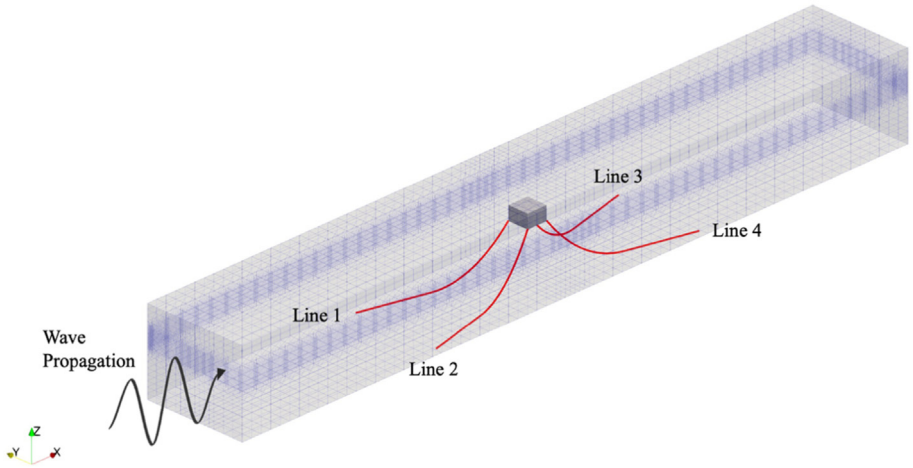

Fig. 3. Grid system and mooring lines of moored floating box.

15, 30 and 60 segments are considered.

The simulations are conducted for up to 14 s, with the adjustable time step size controlled by a maximum Courant number of 0.9. Fig. 4 shows the surge, heave motion, and pitch motions of a moored floating body for different mesh counts, mesh techniques, and mooring line segments. The results with the medium mesh and morphing technique are consistent for all three segments. For the remaining simulation cases, the mooring line is divided into 30 segments. For the surge motion, the two mesh techniques shows similar results, and the results with three meshes shows a similar amplitude and period, and agrees with the experimental data (Wu et al., 2019), while the overset mesh technique shows a reduced amplitude. For the heave motion, both mesh techniques shows similar results. In terms of the pitch motion, the present mesh techniques shows two peaks being predicted when the angle increases, which can also be observed in the results of other researchers (Palm et al., 2016; Domínguez et al., 2019; Chen and Hall, 2022). The present results are slightly delayed compared to the experimental data (Wu et al., 2019). In the amplitude of pitch motion, morphing mesh technique shows better results in defining rotation compared to overset mesh technique. Previous researchers mentioned that the disagreement in pitch motion is due to the uncertainty in the measurements in the experiment (Palm et al., 2016; Chen and Hall, 2022) and discrepancy in the definition of the geometry (Domínguez, et al., 2019). In the simulation, the absence of a plate for camera marker receivers (Wu et al., 2019) attached to the floating body to track its motion causes a difference in the floating body's moment of inertia. Thus, the rotational motions are affected significantly. Fig. 5 shows the meshes

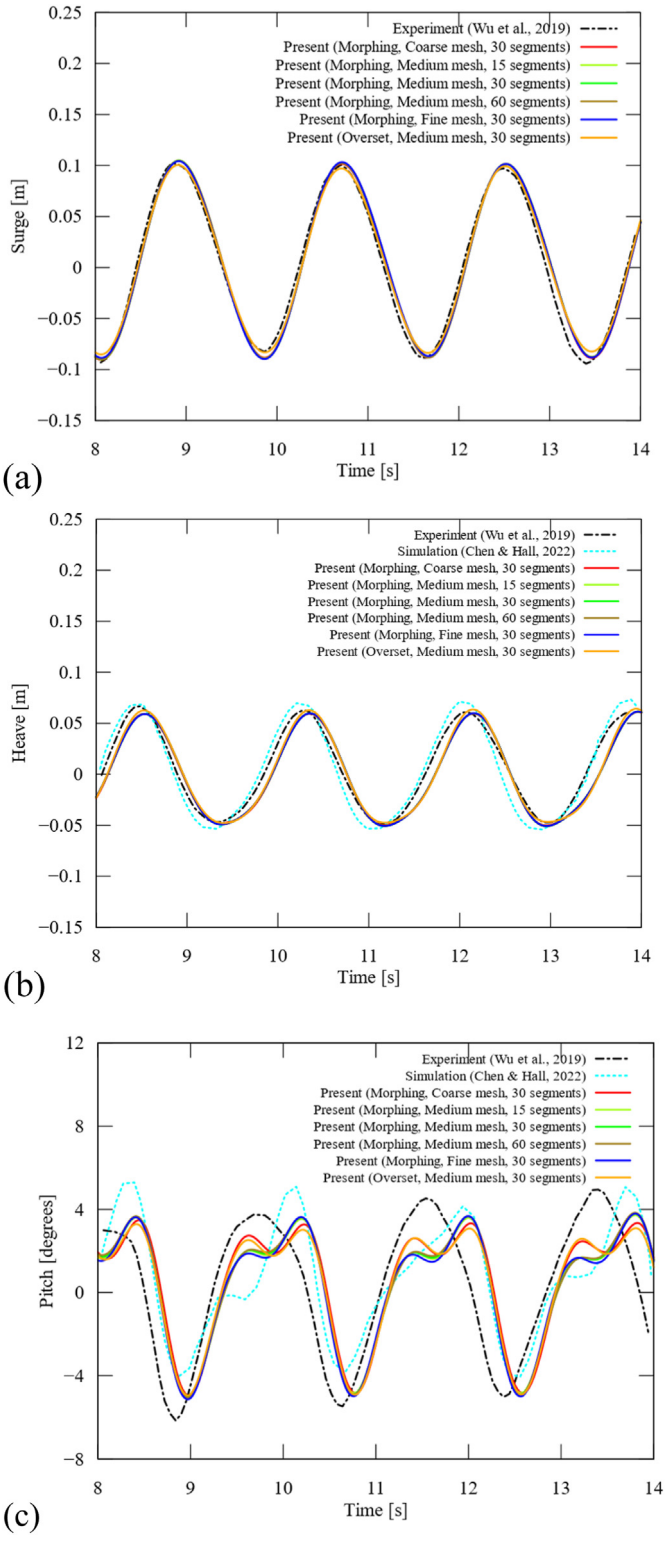

Fig. 4. Moored motions of floating body: (a) surge; (b) heave; (c) pitch.

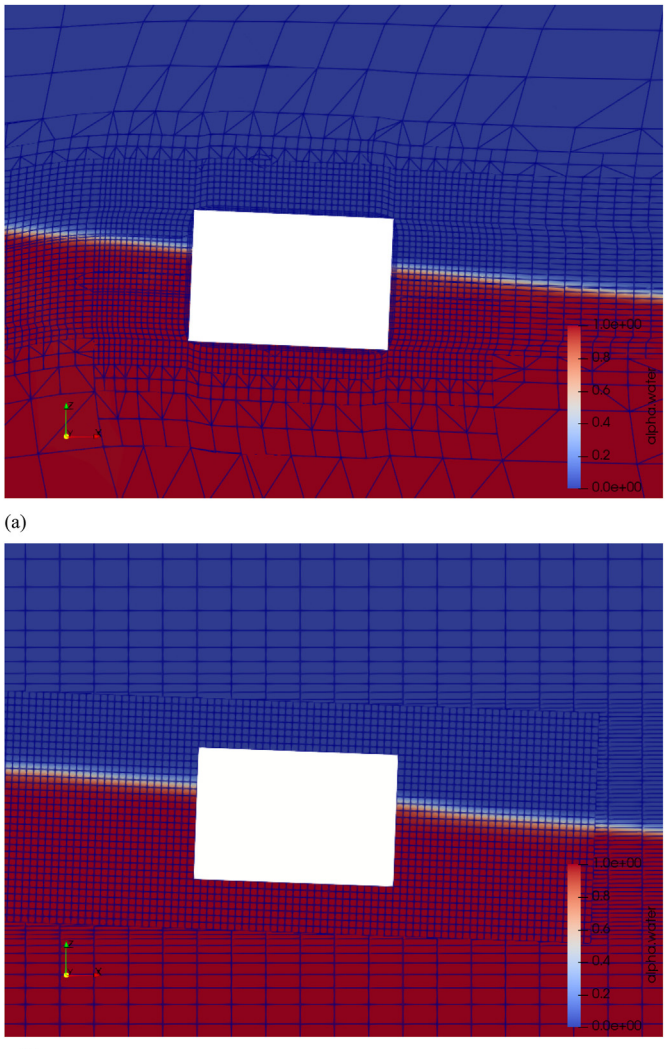

Fig. 5. Meshes around the cubic box: (a) Morphing mesh technique (b) Overset mesh technique.

surrounding the cubic box when the pitch motion reaches its maximum value at 10 s. In the morphing mesh technique, node points closer to the cubic box have large displacements, while those farther away have smaller displacements. In the overset mesh technique, the node points around the cubic box are maintained its topology.

Figs. 6 and 7 show the time series of tension measured at the anchor and fairlead of mooring lines 1 and 3, respectively. Mooring line 1 is located at the front side and the mooring line 3 is installed at the rear side. The obtained mooring line forces of three different mesh configurations show a good similarity. In the experiment, the results suggest that the snap loads cause a higher tension in line 3 compared to line 1. On mooring line 1, the period and amplitude are similar but slightly different from the experimental data. On the other hand, on mooring line 3, the period is similar, but the amplitude is smaller than the experiment. Such discrepancies can be attributed to the limitations of MoorDyn in predicting snap loads, a phenomenon that also is observed in Chen and Hall's (2022) research. On line 3, the vibration observed at low tension is induced by the influence of the seabed model (Lee et al., 2021). Other possible reasons for differences in the results may include errors in estimating line stiffness or empirical hydrodynamic coefficients (e.g., drag, added mass, seabed friction). In detail, in the experiment, the chain ring of the mooring line is connected to the load cell and secured using two tight cable ties (Chen and Hall, 2022). However, MoorDyn is not able to model this type of connection (Domínguez et al., 2019). These differences result in discrepancies in the tension of the mooring line.

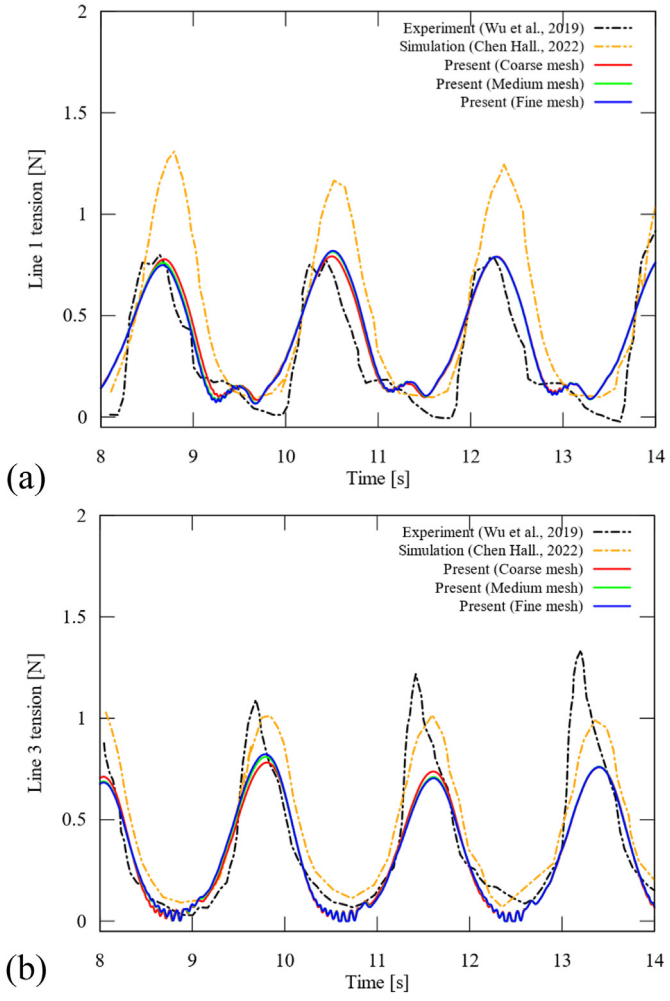

Fig. 6. Mooring line tension at the anchor: (a) Line 1; (b) Line 3.

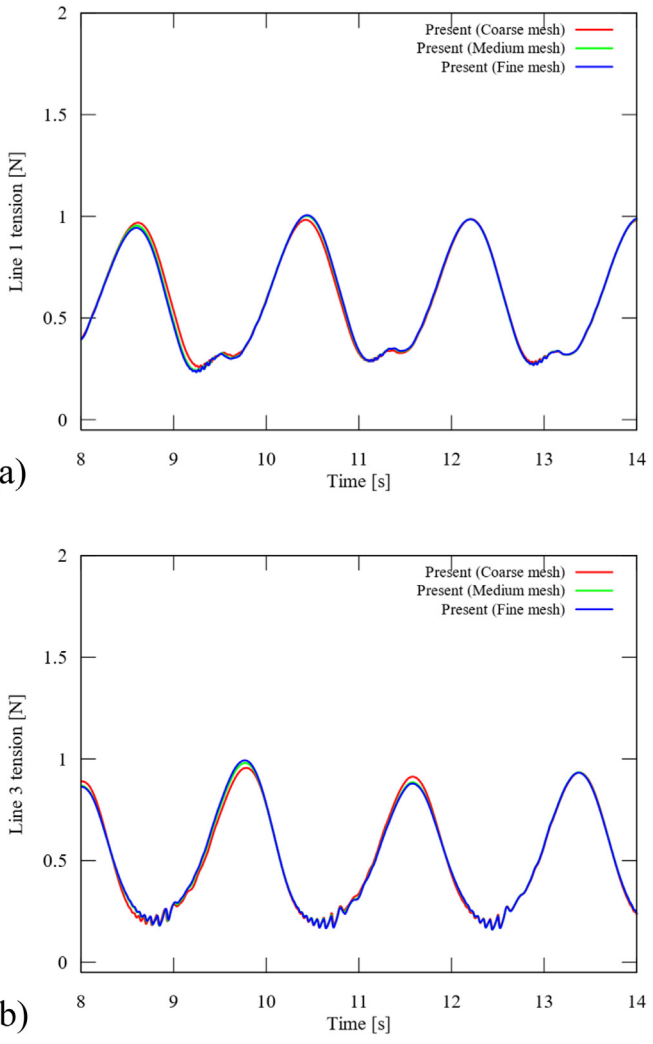

Fig. 7. Mooring line tension at the fairlead: (a) Line 1; (b) Line 3.

Fig. 8 shows the moored floating body in the regular waves. The mooring line tension varies with wave elevations. The wave crest pushes the box backward and produces high tension on lines 1 and 2. The wave trough, on the other hand, pulls the box forward and produces low tension on lines 1 and 2. The tension on lines 1 and 3 is periodically changed with opposite wave phases.

3.2. Moored K-SEMI in waves

Moored motions of a semi-submersible platform in waves are simulated and compared with the experimental data (Nam et al., 2022). The experiments are conducted in a wave tank with a length of 56 m, a width of 30 m, and a depth of 4.5 m. The wavelength of the regular waves considered is 9.79 m, the wave height is 0.04 m, and the wave period is 2.54 s. The model used for the experiment is designed by Korea Research Institute of Ships & Ocean Engineering (KRISO) and is called the KRISO standard semi-submersible platform (K-SEMI). K-SEMI is designed in consideration of operating in a depth of 300 m. In these experiments, a reduced scale model with a ratio of 1/50 is used. The properties of the model are listed in Table 3.

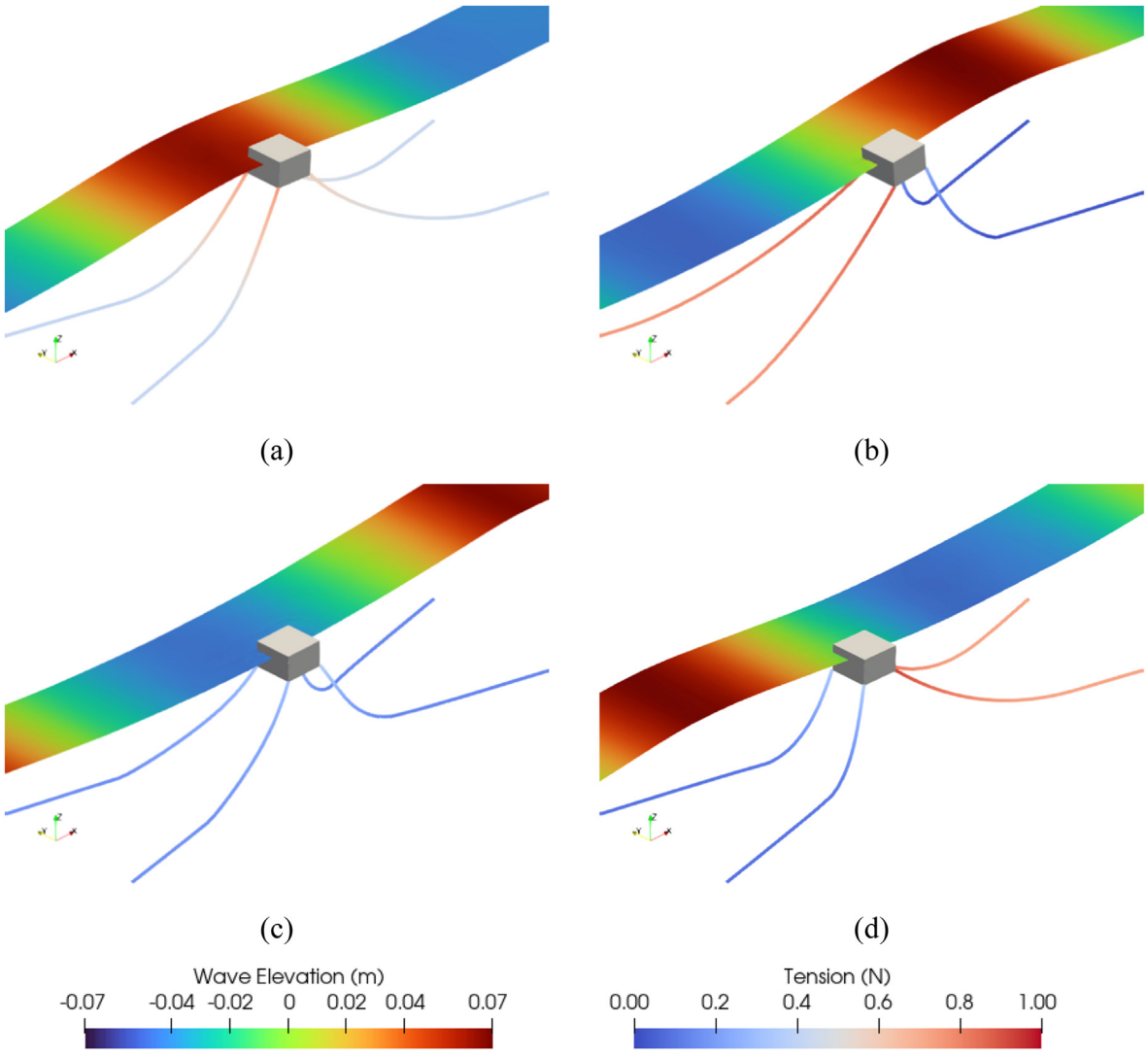

Fig. 8. Mooring line tension and wave elevation around floating body. (a) $t + 1/4T$ (b) $t + 2/4T$ (c) $t + 3/4T$ (d) $t + 4/4T$.

Table 3
Principal particulars of K-SEMI.

Properties	Value	Unit
Scale ratio	1/50	
Pontoon length	2.352	m
Breadth	1.652	m
Draft	0.38	m
Mass	436.8	kg
Mooring line fairlead height from bottom	0.428	m
Moment of inertia of x-axis	194.7	kg • m^2
Moment of inertia of y-axis	198.6	kg • m^2
Moment of inertia of z-axis	300.9	kg • m^2

In Fig. 9, the shape and surface meshes of the K-SEMI model are shown. The mooring lines and computational domain are shown in Fig. 10. A total of 1.3 million meshes are used. The medium mesh with 80 cells per wavelength and 20 cells per wave height is used. The morphing mesh technique is applied to accommodate the body motions. On the K-SEMI surface, the moving wall boundary condition is applied. For the wave generation and to prevent reflection at the boundary, the relaxation zones are applied around the inlet and outlet boundaries, respectively. For the pressure of the top boundary, an open atmosphere condition is applied. For the bottom boundary, a no-slip boundary condition is applied.

The mooring system consisted of 12 catenary chains, and the properties of the mooring lines used in the experiments are listed in Table 4. Mooring lines 1 to 6 are mounted to the back, and lines 7 to 12 are mounted to the front of K-SEMI. The hydrodynamic coefficients of the mooring system are from Hall and Goupee (2015). Each mooring line is discretized into 30 segments.

The simulations are conducted for up to 100 s, with the adjustable time step size controlled by a maximum Courant number of 0.9. All six-degrees-of-freedom motions are allowed during the simulations. The results of the surge, heave, and pitch motions are compared with the results of the experiment, as shown in Fig. 11. After the initial transient response of the simulations, the magnitudes and frequencies of each motion are repeated periodically. The simulation results shows a trend that is very similar to the experimental results in the magnitudes and frequencies of sway, heave, and pitch motions. Fig. 12 shows the forces in the x, y, and z

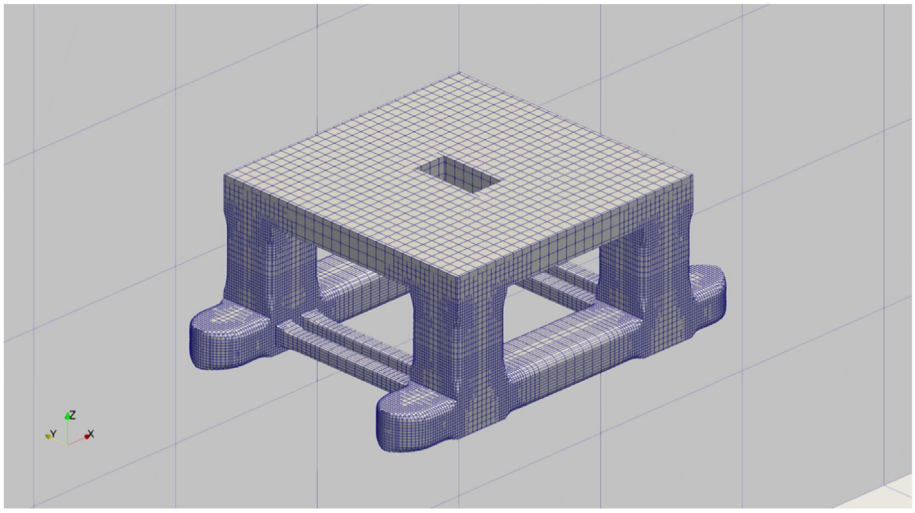

Fig. 9. Surface meshes of K-SEMI.

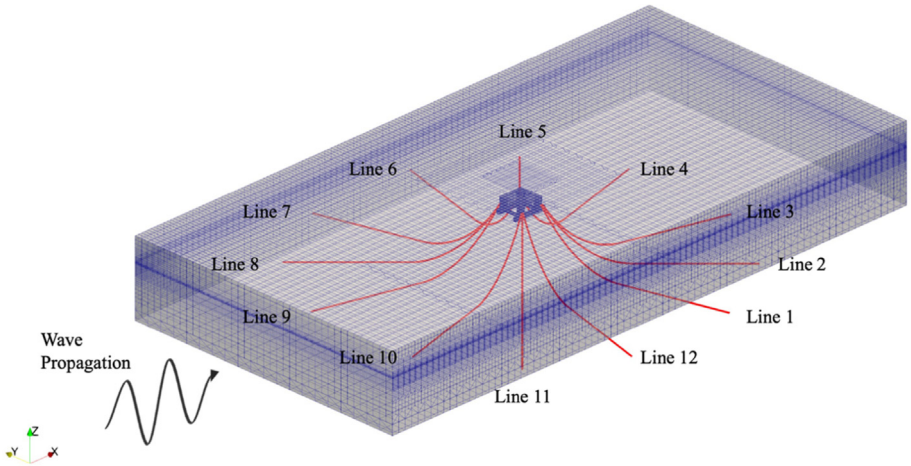

Fig. 10. Mooring lines of K-SEMI.

Table 4
Parameters of mooring line for the K-SEMI simulations.

Properties	Values	Unit
Horizontal span	12.0	m
Vertical span	3.248	m
Total length of the mooring line	13.44	m
Line diameter	4.59	m m
Line weight	0.215	kgf/m
Axial stiffness (*EA*)	1.89×10^4	N

directions acting on the model. The forces acting on the model in the x, y, and z directions are shown in Fig. 12. There is a negligible impact from the y-direction, while the forces in the x and z directions are significant. The x-direction, aligning with the direction of wave propagation, shows the impact of wave forces on driving the structure. The z-direction, associated with the oscillatory motion of the waves, shows the influence of wave-induced motions.

Figs. 13 and 14 show the tension in the mooring line at the anchor and fairlead, respectively. Higher tension is predicted on lines 4 and 9, which are located parallel to the propagation direction of the waves, than on lines 6 and 7, which are located perpendicular to the propagation direction of the waves. Fig. 15 shows the mooring line tension and wave elevation around K-SEMI in one regular wave period. Among the 12 mooring lines, the tension at the fairleads is higher than the tension at the anchor. This is due to the motion of K-SEMI connected to the fairleads and the weight of the mooring lines. The motions of K-SEMI during the cycle of the waves are kept at a low level due to many mooring lines.

4. Conclusions

The motions and mooring system of an offshore platform in regular waves are investigated using a coupled solver of OpenFOAM and MoorDyn. The time marching interface of the previously developed coupled solver has been improved. As a result, the accuracy of a platform which has nonlinear behavior has been improved, and it has become possible to use an adjustable time step calculated from the maximum Courant number. The motion solver class has been modified to define variables and functions related to

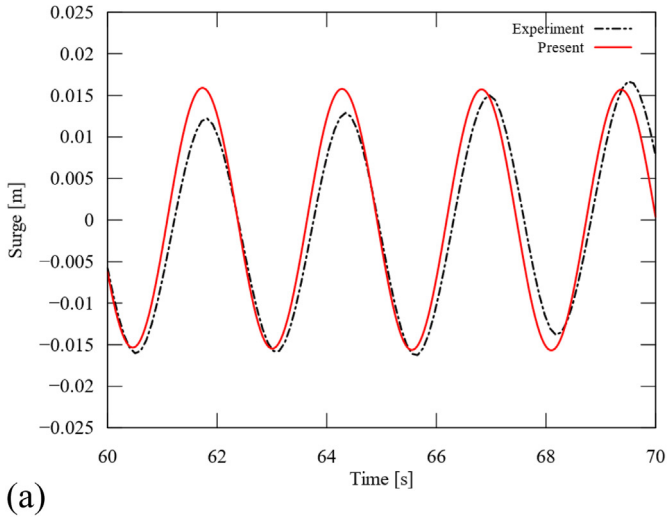

(a)

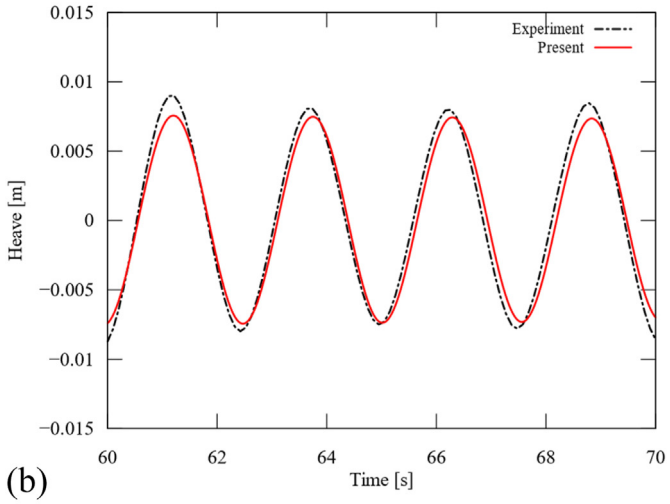

(b)

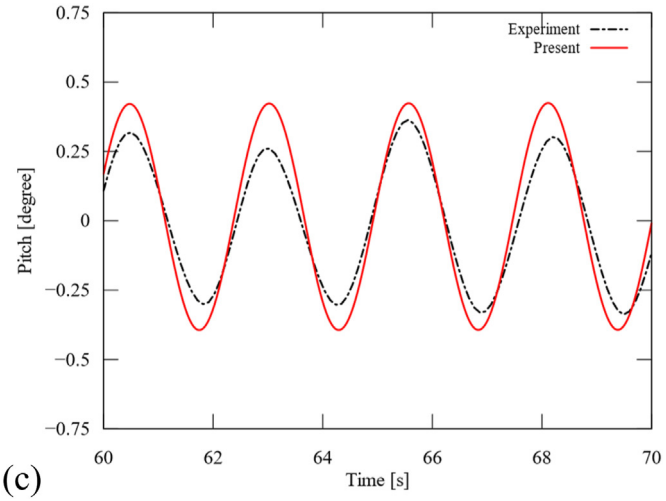

(c)

Fig. 11. Moored motions of K-SEMI: (a) surge motion; (b) heave motion; (c) pitch motion.

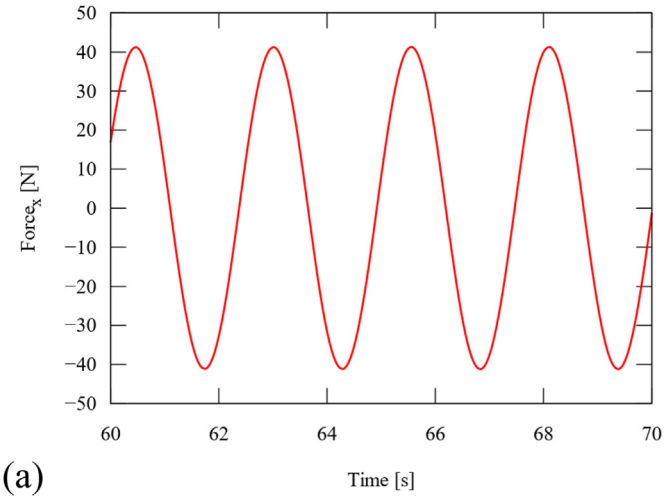

(a)

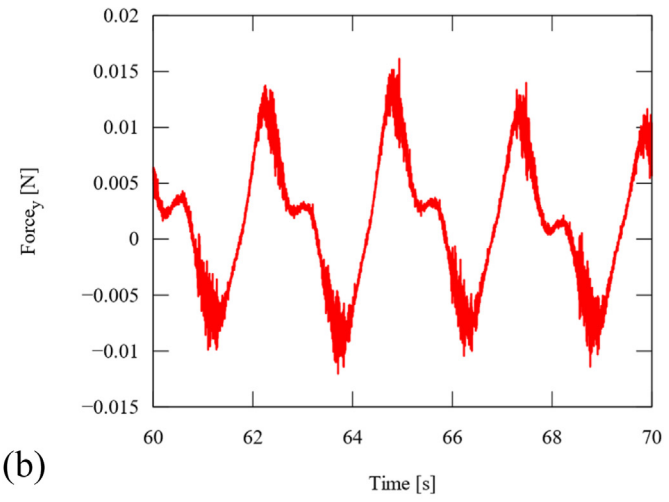

(b)

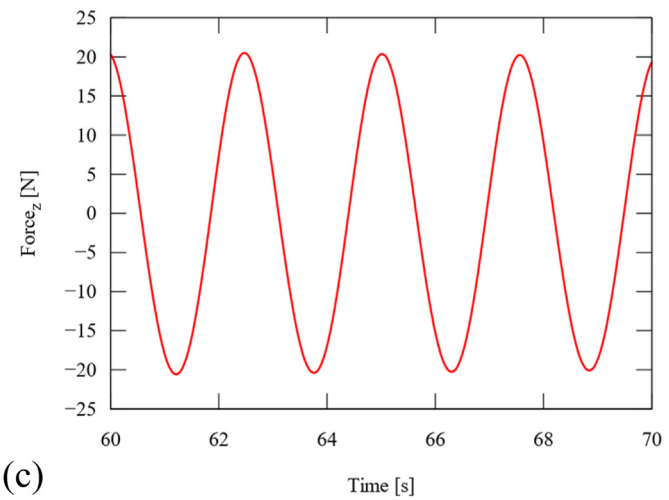

(c)

Fig. 12. Forces acting on K-SEMI: (a) x-direction; (b) y-direction; (c) z-direction.

coupling, thus improving compatibility with the existing solver.

A moored cubic-shaped box in regular waves is simulated for three different meshes, two mesh deformation techniques, morphing mesh and overset mesh, and different mooring line segments. The morphing and overset mesh techniques with different mooring line segments shows similar results to the experimental data in terms of surge and heave motions. In the pitch motion, the present mesh techniques shows a slight delay compared to the experimental data, and shows two peaks when the

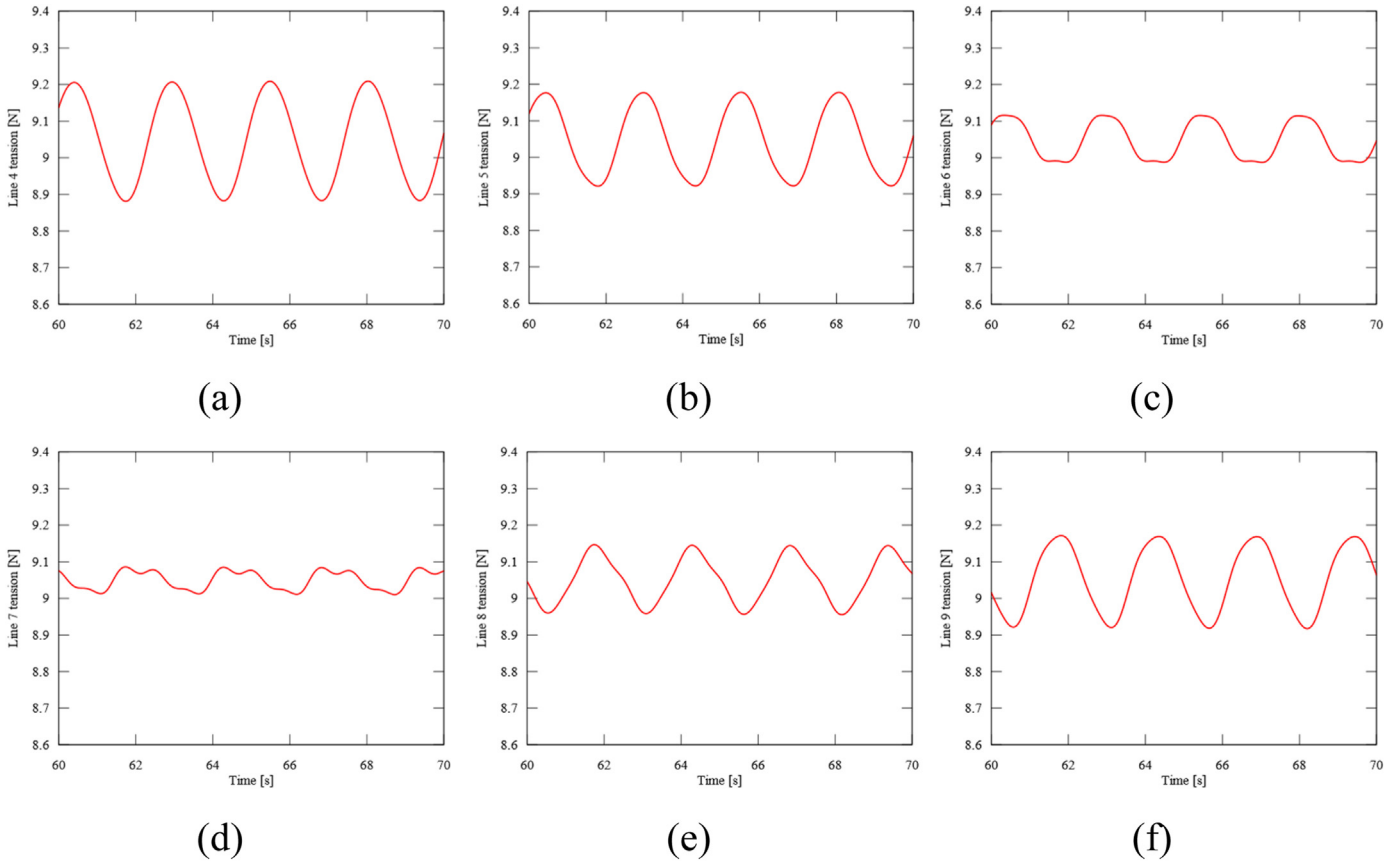

Fig. 13. Mooring line tension at the anchor: (a) Line 4; (b) Line 5; (c) Line 6; (d) Line 7; (e) Line 8; (f) Line 9.

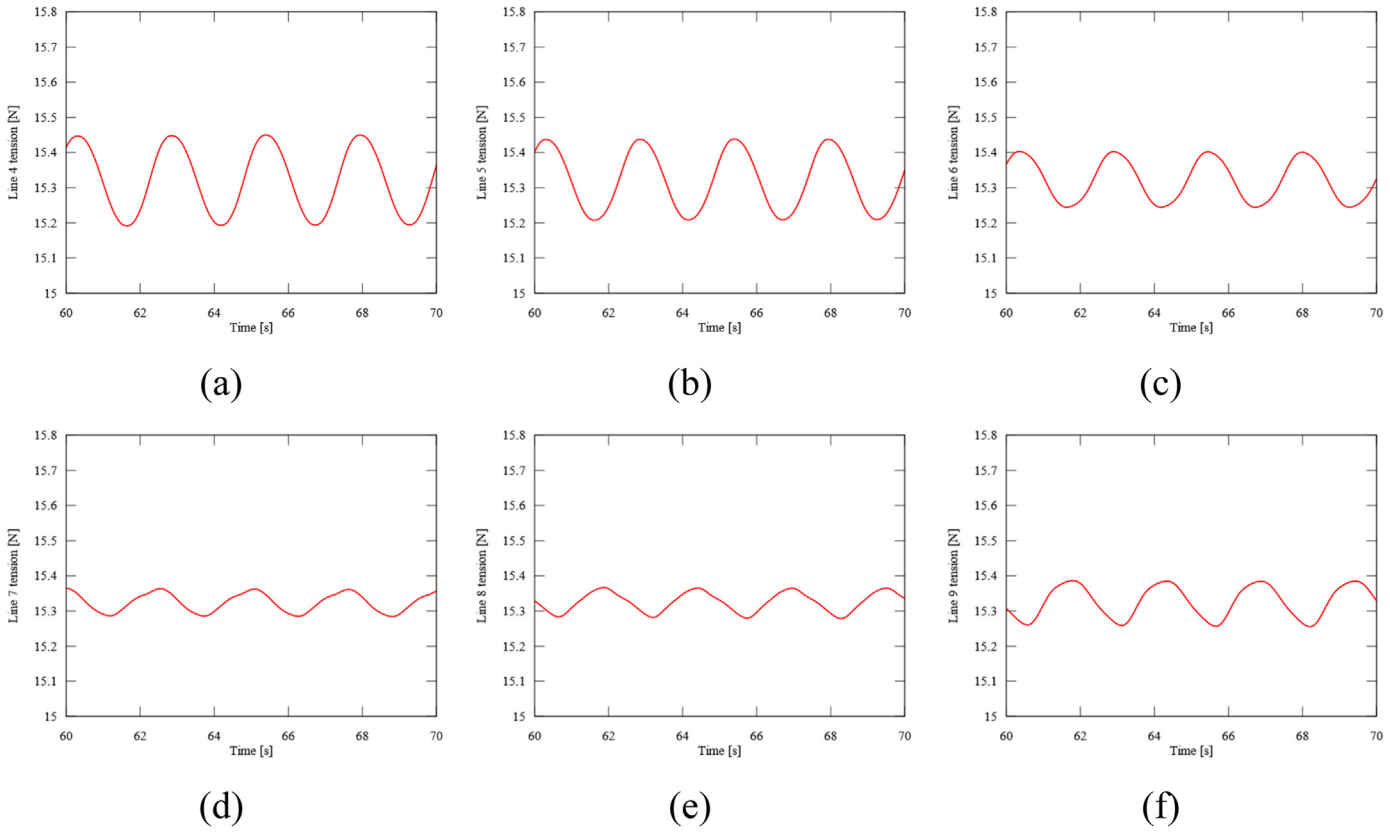

Fig. 14. Mooring line tension at the fairlead: (a) Line 4; (b) Line 5; (c) Line 6; (d) Line 7; (e) Line 8; (f) Line 9.

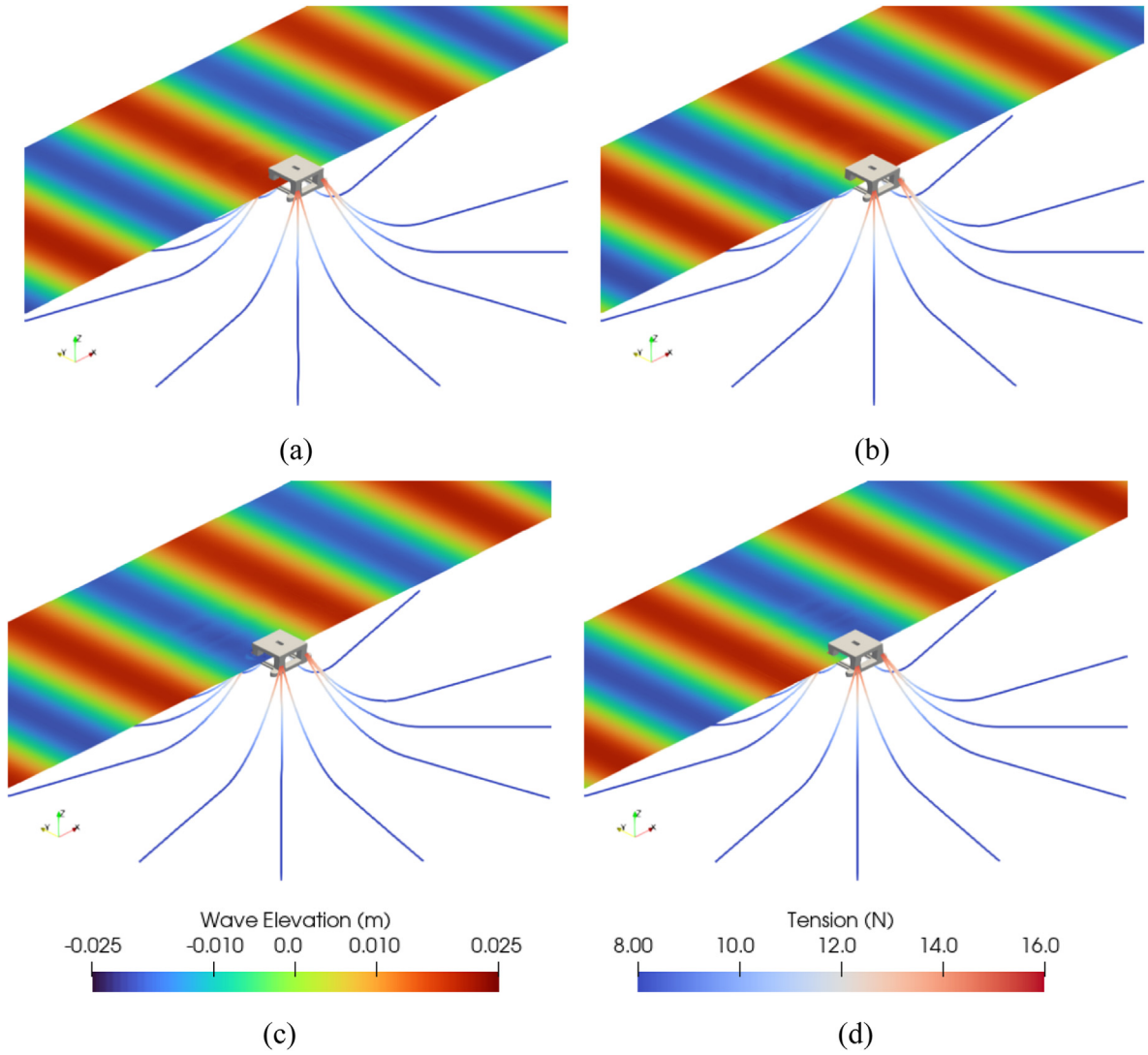

Fig. 15. Mooring line tension and wave elevation around K-SEMI. (a) $t + 1/4T$ (b) $t + 2/4T$ (c) $t + 3/4T$ (d) $t + 4/4T$.

angle increases. The cyclic motions behavior of the floating body being pushed back by the waves and restored to its original position by the tension in the mooring lines is observed.

The motions of K-SEMI with 12-point mooring lines in the regular wave are simulated. The surge, heave, and pitch motions in the simulation results are in good agreement with the experimental results. Significant forces are observed in the x and z directions, corresponding to wave propagation and oscillatory motion, while the y-direction has a negligible impact. The tension in the mooring lines is predicted to be high at the fairlead and low at the anchor. The restoring force of the mooring system, resulting from the tension in the mooring lines, keeps the low-level motion of the K-SEMI model under the regular wave. Using the numerical methods employed in this study, it is expected that the performance of moored structures such as floating wind offshore turbines and wave energy converters and their mooring systems can be evaluated under extreme environmental conditions.

Acknowledgement

This research was supported by the National Research Foundation of Korea (NRF-2021R1I1A3044639) and a part of research program, "Development of CFD technology for global performance analysis of offshore structure (PES4330)" supported by Korea Research Institute of Ships and Ocean Engineering.

Declaration of competing interest

The authors declare that they have no known competing financial interests or personal relationships that could have appeared to influence the work reported in this paper.

References

Aamo, O.M., Fossen, T.I., 2000. Finite element modelling of mooring lines. Math. Comput. Simulat. 53 (4–6), 415–422.
Aliyar, S., Ducrozet, G., Bouscasse, B., Bonnefoy, F., Sriram, V., Ferrant, P., 2022. Numerical coupling strategy using HOS-OpenFOAM-MoorDyn for OC3 Hywind SPAR type platform. Ocean Eng. 263, 112206.
Amaechi, C.V., Odijie, A.C., Wang, F., Ye, J., 2022. Numerical investigation on mooring line configurations of a Paired Column Semisubmersible for its global performance in deep water condition. Ocean Eng. 250, 110572.
Chen, H., Hall, M., 2022. CFD simulation of floating body motion with mooring dynamics: coupling MoorDyn with OpenFOAM. Appl. Ocean Res. 124, 103210.
Choi, Y.M., Bouscasse, B., Ducrozet, G., Seng, S., Ferrant, P., Kim, E.S., Kim, Y.J., 2023. An efficient methodology for the simulation of nonlinear irregular waves in computational fluid dynamics solvers based on the high order spectral method with an application with OpenFOAM. Int. J. Nav. Archit. 15, 100510.

Domínguez, J.M., Crespo, A.J.C., Hall, M., Altomare, C., Wu, M., Stratigaki, V., Troch, P., Cappietti, L., Gómez-Gesteria, M., 2019. SPH simulation of floating structures with moorings. Coast. Eng. 153, 103560.
Ghafari, H., Dardel, M., 2018. Parametric study of catenary mooring system on the dynamic response of the semi-submersible platform. Ocean Eng. 153, 319–332.
Hall, M., Buckham, B., Crawford, C., Nicoll, R.S., 2011. The importance of mooring line model fidelity in floating wind turbine simulations. In: OCEANS'11 MTS/IEEE KONA, pp. 1–8.
Hall, M., Goupee, A., 2015. Validation of a lumped-mass mooring line model with DeepCwind semisubmersible model test data. Ocean Eng. 104, 590–603.
Huang, H., Gu, H., Chen, H.-C., 2022. A new method to couple FEM mooring program with CFD to simulate Six-DoF responses of a moored body. Ocean Eng. 250, 110944.
ITTC, 2014. Recommended procedures and guidelines. "Practical Guidelines for Ship CFD Application" 7, 5-03-02-03.
Jasak, H., 2009. OpenFOAM: open source CFD in research and industry. Int. J. Nav. Archit. 1, 89–94.
Jiang, C., el Moctar, O., 2022. Extension of a coupled mooring–viscous flow solver to account for mooring–joint–multibody interaction in waves. J. Ocean Eng. Mar. Energy.
Khan, N.U., Ansari, K.A., 1986. On the dynamics of a multicomponent mooring line. Comput. Struct. 22 (3), 311–334.
Kim, H., Park, S., 2021. Coupled level-set and volume of fluid (CLSVOF) solver for air lubrication method of a flat plate. J. Mar. Sci. Eng. 9 (2), 231.
Kwon, C.S., Yeon, S.M., 2023. CFD study to predict the effect of a passing ship on moored ships in a confined waterway. Int. J. Nav. Archit. 15, 100527.
Lee, S.C., Song, S., Park, S., 2021. Platform motions and mooring system coupled solver for a moored floating platform in a wave. Processes 9 (8), 1393.
Liu, Y., Xiao, Q., Incecik, A., Peyrard, C., Wan, D., 2017. Establishing a fully coupled CFD analysis tool for floating offshore wind turbines. Renew. Energy 112, 280–301.
Liu, B., Park, S., 2023. CFD simulations of the effects of wave and current on power performance of a horizontal axis tidal stream turbine. J. Mar. Sci. Eng. 11, 425.
Nam, H.-S., Park, D.-M., Cho, S.K., Hong, S.Y., 2022. Analysis of relative wave elevation around semi-submersible platform through model test: focusing on comparison of wave probe characteristics. J. Ocean Eng. Technol. 36 (1), 1–10.
Palm, J., Eskilsson, C., Paredes, G.M., Bergdahl, L., 2016. Coupled mooring analysis for floating wave energy converters using CFD: formulation and validation. Int. J. Mar. Energy 16, 83–99.
Park, S., Park, S.W., Rhee, S.H., Lee, S.B., Choi, J.-E., Kang, S.H., 2013. Investigation on the wall function implementation for the prediction of ship resistance. Int. J. Nav. Archit. Ocean Eng. 5 (1), 33–46.
Rinaldi, G., Gordelier, T., Sansom, M., Johanning, L., 2021. Development of a modular mooring system with clump weights. Ocean Eng. 223, 108536.
Thomsen, J.B., Ferri, F., Kofoed, J.P., 2017. Screening of available tools for dynamic mooring analysis of wave energy converters. Energies 10 (7), 853.
Tian, C., Liu, M., Xiao, L., Lu, H., Wang, J., 2021. Numerical studies on flow-induced motions of a semi-submersible with three circular columns. Int. J. Nav. Archit. Ocean Eng. 13, 559–616.
Weiss, J.M., Maruszewski, J.P., Smith, W.A., 1999. Implicit solution of preconditioned Navier-Stokes equations using algebraic multigrid. AIAA J. 37 (1), 29–36.
Wu, M., Stratigaki, V., Troch, P., Altomare, C., Verbrugghe, T., Crespo, A., Cappietti, L., Hall, M., Gómez-Gesteira, M., 2019. Experimental study of a moored floating oscillating water column wave-energy converter and of a moored cubic box. At. Energ. 12 (10), 1834.
Yang, Y., Bashir, M., Li, C., Wang, J., 2021. Investigation on mooring breakage effects of a 5 MW barge-type floating offshore wind turbine using F2A. Ocean Eng. 233, 108887.